Analytical Modeling and Design Optimization of a Vernier Permanent Magnet Motor

Wang, Bingnan; Zhou, Lei; Wang, Hongyu; Lin, Chungwei

TR2021-124   October 20, 2021

Abstract

In this paper, we present the analysis and design optimization of a Vernier permanent magnet (VPM) motor for direct-drive applications. A subdomain-based analytical model is developed for fast calculation of the electromagnetic performances, including air-gap flux, torque ripple, and power factor. Built on the analytical model, we investigate the trade-off between torque generation and power factor of the VPM motor, and conduct multi-objective optimization for key design parameter of the VPM motor. Flux density in different regions of the stator core is calculated from the analytical model, on which a constraint is set in the objective functions to consider the saturation effect. The optimized VPM achieves 1.9x torque output compared with a commercially-available surface-mount permanent magnet direct-drive motor with the exact inner and outer dimensions at the same speed.

IEEE Energy Conversion Congress and Exposition (ECCE) 2021

Analytical Modeling and Design Optimization of a Vernier Permanent Magnet Motor

Bingnan Wang[1], Lei Zhou[1,2], Hongyu Wang[1], and Chungwei Lin[1]

[1] Mitsubishi Electric Research Laboratories, 201 Broadway, Cambridge, MA 02139, USA
[2] Department of Mechanical Engineering, The University of Texas at Austin, Austin, TX, USA

Abstract—**In this paper, we present the analysis and design optimization of a Vernier permanent magnet (VPM) motor for direct-drive applications. A subdomain-based analytical model is developed for fast calculation of the electromagnetic performances, including air-gap flux, torque ripple, and power factor. Built on the analytical model, we investigate the trade-off between torque generation and power factor of the VPM motor, and conduct multi-objective optimization for key design parameters of the VPM motor. Flux density in different regions of the stator core is calculated using the analytical model, based on which a constraint is set in the objective functions to take the saturation effect into account. The design optimization process is implemented for a multi-objective optimization of the VPM motor. The optimized machine achieves over 1.8× torque output compared with a commercially-available surface-mount permanent magnet direct-drive motor with the exact inner and outer dimensions at the same operating speed.**

Index Terms—**Vernier permanent magnet motor, magnetic field modeling, design optimization.**

I. INTRODUCTION

Direct-drive machines are attractive for many applications due to the benefits brought by the elimination of mechanical transmission elements such as gearboxes and belts, including high dynamic performance, high position accuracy, high torque density, etc. The increasing demands from a few emerging industries, such as robotics and electric vehicles, have inspired recent innovations on direct-drive motor technologies. Surface-mount permanent magnet (SMPM) motor is one of the dominating topologies and has been applied in existing direct-drive motor products, due to the high torque density it can produce [1]. On the other hand, Vernier permanent magnet (VPM) motor, which combines magnetic gearing effect and a regular permanent magnet motor, shows the potential of producing even higher torque density at low speed range thanks to the magnet gearing effect, and has been investigated extensively in recent years for various direct-drive applications [2], [3], [4].

For the analysis of electric machines, finite-element method (FEM) based simulation tools are now quite sophisticated after decades of development, and have been widely used by motor designers and researchers. However, due to the computationally-intensive and time-consuming nature of the method, FEM simulations are often not suitable for the design optimization of new motors, where a large number of design parameters need to be tuned. Analytical methods have the potential to fill the gap with good balance of

accuracy and calculation speed. In particular, subdomain method solves for the partial differential equation (PDE) of a magnetic potential derived from Maxwell's equations, and finds analytical solutions using Fourier analysis techniques, and is proven to be the most accurate analytical method [5], [6]. With the subdomain method, the slotting effect can be accounted for at any rotor position, and both open-circuit and on-load fields can be calculated. Therefore the electromagnetic performances, including the torque waveform at different operating conditions, can be obtained with good accuracy. The method has been developed for the rapid analysis of various machine types, including surface mount permanent magnet motors, switched reluctance motors, interior permanent magnet motors, and Vernier motors [7], [8], [9].

In this work, we present a motor design optimization process using subdomain method and apply it to the design analysis and optimization of a radial-flux VPM direct-drive motor with a space-saving large hollow shaft, which is desirable to allow cabling and piping to pass through. Compared with convention SMPM motor based design with exactly the same inner and outer dimension, we expect VPM motor to have higher torque generation capability at the same operating speed. We present the subdomain based analytical model for the rapid analysis of the VPM machine, including the air gap flux, the back-EMF, the power factor, and the torque generation, and validate the results with nonlinear FEM simulations. While nonlinear effect of the ferromagnetic material in the motor is not explicitly included in the calculation, the saturation effect is considered in the model by setting threshold values for the calculated flux density in the core regions, and motor designs with flux density higher than the threshold are discarded during the optimization process. A known drawback of VPM motor is the relatively lower power factor. In the paper, we investigate the trade-off between the torque generation capability and the power factor of the VPM motor, and demonstrate the motor optimization process using the analytical model with a multi-objective optimization to find the Pareto front of torque and power factor of the VPM motor.

The rest of the paper is organized as follows: we first discuss the working principle and compare with the conventional SMPM. We then describe the modeling process of the VPM, and the optimization setup. We then present the performance of the optimized VPM design. In the last section, we conclude the paper and lay out future work.
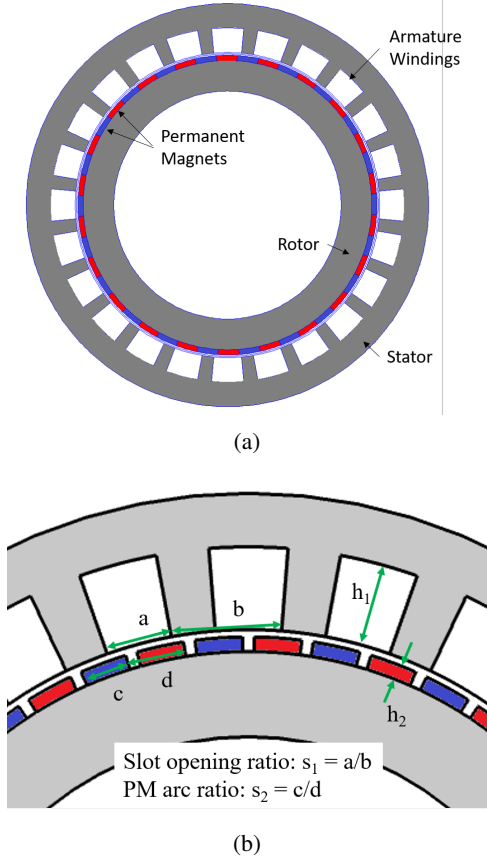
(a)

Slot opening ratio: $s_1 = a/b$
PM arc ratio: $s_2 = c/d$

(b)

Fig. 1: (a) The structure of a radial-flux VPM motor. (b) Close-up view with key geometrical parameters defined.

II. THE PROPOSED DESIGN ANALYSIS AND OPTIMIZATION METHOD

In this section, we first introduce the principle and topology of the VPM motor, and then lay out the proposed analytical calculation and optimization process for the design of the machine.

A. The VPM Motor Design

The topology of the radial-flux VPM motor is illustrated in Fig. 1. A VPM is considered as a type of flux-modulation machine, and can be viewed as a combination of a conventional PM machine and a magnetic gear, where the PM generated magnetic field interacts with the modulated stator spatial harmonics due to the teeth to generate torque. To achieve that, the combination of stator teeth number Z_s, rotor pole pair number Z_r, and stator winding pole-pair number p has to satisfy $Z_r = Z_s \pm p$; this way the air gap flux harmonic of the order Z_r is produced from the stator-generated magneto-motive force (MMF) modulated by the stator teeth, which can then interact with the rotor PM generated magnetic field of the same harmonic order to generate torque.

B. The Analytical Model

We calculate the magnetic field and subsequently the electromagnetic performance metrics of the VPM motor using semi-analytical subdomain method. In order to obtain analytical solutions, a few simplifications are made for the motor model: (a) End effect in the axial direction is neglected; (b) The model is constructed in 2D polar coordinates, and only allows structures of the magnets and the slots to be ring-shaped sections; (c) The magnets are magnetized in the radial direction; (d) The iron core is assumed to be infinitely permeable. Due to the high number of slots and magnets in the VPM motor, the geometrical simplifications have very small influence on the calculation accuracy, as compared with VPM motor with rectangular-shaped magnets and slots. The simplified motor domain is divided into separate subdomains, with region I to model the PMs, region II to model the air gap region, and region III to model the slots.

A governing PDE of magnetic vector potential for each subdomain $\mathbf{A}$, which is defined as $\nabla \times \mathbf{A} = \mathbf{B}$, where $\mathbf{B}$ is the magnetic flux density, is derived from Maxwell's equations: $\nabla^2 \mathbf{A} = -\mu_0 (\mathbf{J} + \nabla \times \mathbf{M})$, where $\mathbf{J}$ is current density for slot region, and $\mathbf{M}$ is the PM magnetization, and both sources can be expressed in the form of Fourier series. For air gap region, the right hand side is 0. Closed-form solutions can be obtained for each region with Fourier analysis.

For the PM region, the solution to the governing Poisson's equation is written as

$$A_z^I(r,\theta) = A_o^I + B_o^I \ln r$$
$$+ \sum_{n=1}^{\infty} \left[\begin{array}{c} \left(A_n^I r^{-n} + B_n^{II} r^n + W_n(r) \right) \sin n\theta \\ + \left(C_n^I r^{-n} + D_n^I r^n - W_n(r) \right) \cos n\theta \end{array} \right] \tag{1}$$

where the integer n represents the harmonic order of the Fourier series, and W_n represents the contribution from the PM magnetization.

For the air gap domain II, the solution to the governing Laplace's equation takes the form of

$$A_z^{II}(r,\theta) = A_0^{II} + B_0^{II} \ln r$$
$$+ \sum_{n=1}^{\infty} \left(A_n^{II} \left(\frac{r}{r_3} \right)^{-n} + B_n^{II} \left(\frac{r}{r_4} \right)^{n} \right) \sin n\theta$$
$$+ \sum_{n=1}^{\infty} \left(C_n^{II} \left(\frac{r}{r_3} \right)^{-n} + D_n^{II} \left(\frac{r}{r_4} \right)^{n} \right) \cos n\theta \tag{2}$$

where r_3 and r_4 represents the inner and outer radius of the air gap respectively.

For the slot domain III, the vector potential is governed by Poisson's equation of the form $\nabla^2 \mathbf{A} = -\mu_0 \mathbf{J}$, where $\mathbf{J}$ is the surface current density in the region. The solution is expressed as

$$A_z^{III,i}(r,\theta) = A_0^{III,i} + B_0^{III,i} \ln r - \mu_0 J_z^{III,i} r^2/4$$
$$+ \sum_{v=1}^{\infty} \left(A_v^{III,i} \left(\frac{r}{r_4} \right)^{-v} + B_v^{III,i} \left(\frac{r}{r_5} \right)^{v} \right) \cos[k_v(\theta - \delta_i)] \tag{3}$$

where i represents the i-th slot, and δ represents the starting angular position of the slot opening, and $k_v = v\pi/a$ with a the angular width of the slot.

After establishing the general form of vector potential solutions in each domain, boundary conditions between neighboring domains are utilized in order to fully identify the unknown coefficients in the Fourier series. A system of linear equations can be set up from these boundary conditions, and the full solution of magnetic potential can be obtained after solving for the equations. The electromagnetic performance metrics, such as magnetic flux density, flux linkage, induced voltage, and torque waveform, can be calculated subsequently.

The flux linkage is obtained from the magnetic vector potential using Stokes' theorem. First the flux linkage associated with each stator slot is calculated

$$\phi = \int_S \mathbf{B} dS = \oint_l \mathbf{A} dl, \tag{4}$$

where S is the surface of the slot, and l is its boundary. Then the total flux linkage of each phase is calculated by summing all contributions from the phase winding. The back-EMF is then obtained with $E_a = -d\phi/dt$.

The torque is calculated from the air gap flux using Maxwell stress tensor method

$$T = \frac{l_k r^2}{\mu_0} \int_0^{2\pi} B_{rg} B_{\theta g} d\theta = \frac{l_k r^2}{\mu_0} \sum_{n=1}^{N} (B_{rc} B_{\theta c} + B_{rs} B_{\theta s}), \tag{5}$$

where r is the radius of the air gap, B_{rg} and $B_{\theta g}$ are the radial and tangential flux density in the air gap, respectively, and the subscripts c and s denote the cosine and sine components of the flux harmonics, respectively. The torque waveform can be obtained by repeating the calculation process at each rotor position. Since the relative position of the slots and the magnets is updated for each calculation, the slotting effect at each rotor position can be more accurately accounted for than other analytical based models such as relative permeance model, which adopts the same permeance function to account for the slotting effect for any rotor position. Therefore, the torque waveforms, including the cogging torque at no-load condition and the torque ripple at on-load conditions, can be calculated with good accuracy.

Low power factor is a major drawback of VPM motors due to the high stator pole pitch compared to the rotor pole pitch. Consequently, a significant portion of the magnetic flux generated by the permanent magnets does not contribute to the flux linkage, making the induced voltage low; on the other hand, the winding inductance is relatively high. Based on the analytical subdomain method, we are also able to obtain the inductance and the power factor of the VPM motor. By exciting only one phase winding with phase current I_a, we run the subdomain calculation, and obtain the magnetic vector potential in the slots. The magnetic energy stored in the system is calculated using

$$W_m = \frac{1}{2} l_k \int \mathbf{A} \cdot \mathbf{J} dS, \tag{6}$$

where l_k is the stack length of the motor, $\mathbf{J}$ is the current density in the slot. The integration is calculated for each individual slot, and the total magnetic energy is the summation over all the slot domains. The self-inductance of the phase winding is then obtained by

$$L_a = 2W_m^2/I_a^2, L_a = 2W_m/I_a^2, (no \, square??) \tag{7}$$

where I_a is the phase current.

To calculate the power factor, we assume the motor works at maximum torque condition with zero d-axis current; the winding resistance is also neglected for simplification. The power factor of the machine is calculated by the ratio of the back-EMF and the phase voltage

$$PF = E_a/V_s = E_a/\sqrt{E_a^2 + (\omega_e L_a I_a)^2}, \tag{8}$$

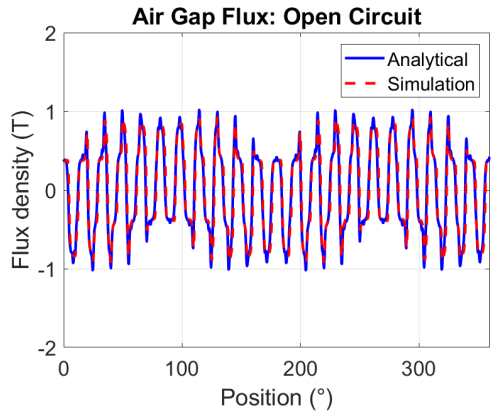where ω_e is the electrical angular speed.

III. MODEL VALIDATION AND ANALYSIS

In this work, we demonstrate the VPM motor design and optimization process, and compare the VPM motor performance with a commercially available SMPM direct-drive motor (Mitsubishi Electric TM-RB series) with the same inner and outer dimensions, whose rotor inner diameter is 130 mm, stator outer diameter is 230 mm, air gap length is 1.5 mm, and the stack length is 100 mm. The rated torque for the benchmark SMPM motor with liquid cooling is 150 N·m, and the rated speed is 200 rpm.
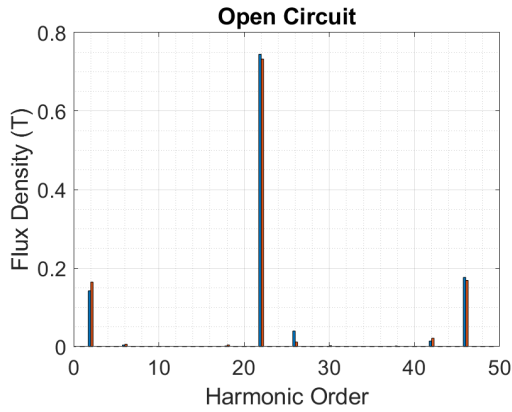
TABLE I: Geometrical Parameters of the VPM Motor

Parameter	Value
Stator pole pair number p	2
Rotor pole pair number Z_r	22
Stator slot number Z_s	24
Stack length (mm)	130
Stator outer diameter (mm)	230
Stator inner diameter (mm)	174
Air gap length (mm)	1.5
Rotor outer diameter (mm)	171
Rotor inner diameter (mm)	130
Rotation speed (rpm)	200

For the VPM motor design, we choose $Z_r = 22$, $Z_s = 24$, and $p = 2$, so that $Z_r = Z_s - p$. The major parameters of the VPM motor are listed in Table I. Three-phase distributed winding is adopted in the slots with filling ratio of 50% and peak current density 10 A/mm^2. All calculations are done at the same rated speed of 200 rpm.
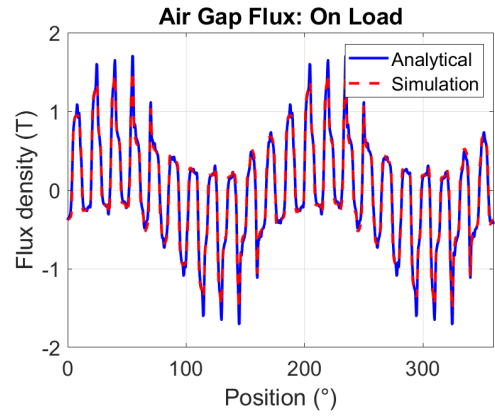
Fig. 2: Comparison between analytical model and FEM simulation of the air-gap flux in radial direction at open-circuit condition: (a) spatial distribution and (b) spectrum components.
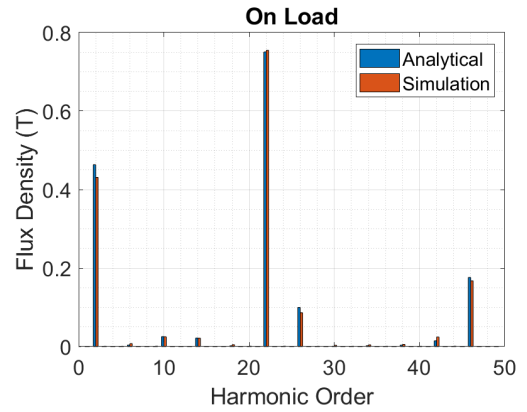
Fig. 3: Comparison between analytical model and FEM simulation of the air-gap flux in radial direction at on-load condition: (a) spatial distribution and (b) spectrum components.

A. Model Validation

We first validate the accuracy of the subdomain based analytical model by comparing the calculation results with nonlinear FEM simulations. The design parameters for the machine to be optimized, as defined in Fig. 1(b), are chosen to be: slot-opening ratio $s_1 = 0.6$, slot depth $h_1 = 15$ mm, PM arc ratio $s_2 = 1$, PM thickness $h_2 = 3$ mm.

We first check the air gap flux distribution of the example VPM motor design obtained from the analytical model, and compare with FEM results. Fig. 2 shows the radial air-gap flux distribution for open-circuit condition. Both the spatial distribution and the amplitude of the spectral components agree well with the FEM simulation results, and the dominating harmonic order is 22, which is the rotor pole pair number Z_r, as expected. Fig. 3 shows the air-gap flux distribution for on-load conditions, and both the spatial distribution and the spectrum components agree well with FEM results. From Fig. 3(b) we can see that the torque generating orders $p = 2$, $Z_s - p = 22$, and the higher $2Z_s - p = 46$ are the dominating components, and the other harmonics that contribute to the torque ripple are small,

suggesting that the machine has very small torque ripple even for this conventional VPM motor without special design measures. This is verified by the torque waveform calculation result as shown in Fig. 4, where the torque ripple is less than 1%. For the on-load calculations, a sinusoidal current waveform with peak current density of 10 A/mm^2 is assumed for the stator winding excitation, and the torque waveform over one electric cycle is plotted. Note that the calculated torque is over 225 N·m, or 150% as compared with the benchmark SMPM motor. In addition, the difference between analytical model and FEM for average torque is less than 2%, and the accuracy is achieved with calculation speed over 10× faster than FEM simulations.

B. Power Factor

Based on the method introduced in the previous section, we calculate the power factor of the VPM motor as well. We keep all the design parameters used for the model validation, and change the slot opening ratio s_1. For each case, we calculate the average torque and power factor of the motor, and the results are shown in Fig. 5. As you can see the power factor
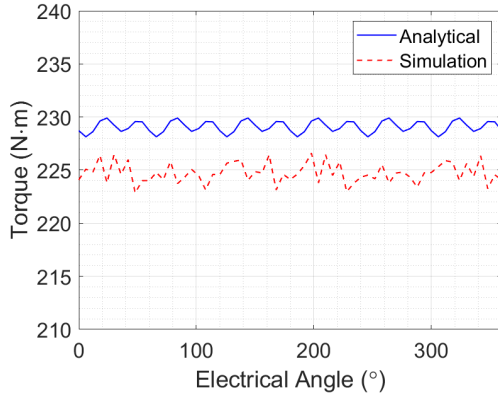
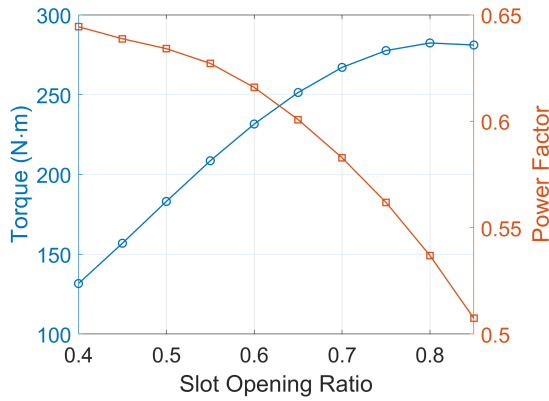Fig. 4: Comparison between analytical model and FEM simulation of the torque generation.

Fig. 5: The calculated electromagnetic torque and power factor of the motor as function of slot opening ratio.

of the VPM machine is low, and there is a trade-off between torque generation and power factor. With the same current density in the slot and filling ratio, when the slot opening ratio s_1 is larger, higher phase current is expected, which leads to higher torque generation; on the other hand, that means larger number of turns to fill the slots and higher inductance, which leads to lower power factor, as indicated in (8). Since power factor needs to be considered to identify the power supply and motor drive requirements, it is therefore desirable to include in the design and optimization process.

IV. THE OPTIMIZATION PROCESS

After establishing the analytical calculation process, we implement the model for design optimization.

A. Saturation Effect

In the analytical calculation process, the iron core is assumed to be infinitely permeable. However the actual core material is nonlinear, and can saturate under high armature reaction field. When saturation happens, the torque generation will be reduced if the current density is kept the same, causing discrepancy between the analytical model and the nonlinear

FEM simulation and actual machine performance. To account for saturation, we calculate the average flux density in the stator teeth region and yoke region with $B_t = \phi_t/A_t$ and $B_y = \phi_y/A_y$, where ϕ_t and ϕ_y are the flux in each region calculated from slot vector potential, and A_t and A_y are the cross-sectional area of the two regions. We record the flux density values for all rotor positions over one electrical cycle, and compare the maximum values with a threshold value.

The magnetic flux density threshold value depends on the magnetic property of the steel selected for the motor core. For high grade cobalt iron, such as Hiperco-50 with high saturation flux density, the threshold value $B_m = 2$ T is used. When the flux density is higher than the threshold, the stator core is considered as over saturated, and the particular motor design is discarded from the optimization process. This consideration is included in the corresponding objective functions of the optimization routine by adding a large weight to the objective when the flux density is above the threshold.

B. Design Optimization Process

With the above considerations, we establish an optimization routine for motor design using the analytical model. A flow chart for the process is described in Fig. 6. For a given set of design parameters, the analytical models is applied to compute the required motor performance metrics, such as magnetic flux density, average torque, torque ripple, and power factor. The stator core flux densities are also calculated and compared with the preset threshold value. If the flux density values are above the threshold, the stator is saturated at the given operating condition, and the motor design is discarded. Otherwise, the objective functions are evaluated based on the calculated motor performance metrics and fed to the optimization algorithm, which determines the next set of design parameters to be evaluated and generate the pareto front of the multi-objective optimization.
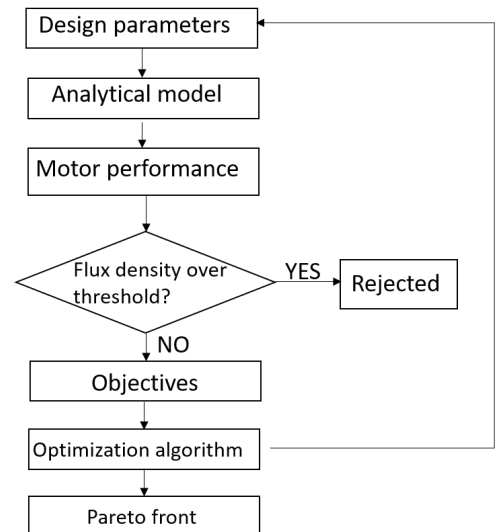

Fig. 6: The proposed design optimization process.

$$\min_x \begin{bmatrix} f_1(x) & = -w_1 T_{avg}(x) + w_2 H[B_{tm}(x) - B_m] + w_3 H[B_{ym}(x) - B_m], \\ f_2(x) & = -w_4 PF(x) + w_5 H[B_{tm}(x) - B_m] + w_6 H[B_{ym}(x) - B_m] \end{bmatrix} \tag{9}$$
$$\text{s.t.} \quad x_{lb} \le x \le x_{ub},$$

where x is the vector of geometrical parameters to be optimized, x_{lb} and x_{ub} are the lower and upper bounds of these parameters respectively, T_{avg} is the average torque over one electrical cycle, B_{tm} and B_{ym} are he maximum value of teeth and yoke flux density respectively. Instead of setting the magnetic flux as constraints, we add the additional terms of Heaviside step functions $H[\cdot]$ in the objective functions, with w_i the weighting assigned to each term. When the flux densities are below the threshold, the additional terms have no contribution to the objectives; when any flux density is above the threshold, a large positive value is added to the objective, effectively rejecting the design.

TABLE II: Parameters to be optimized

Parameters to be optimized	Range
Slot opening ratio s_1	0.5 - 0.8
PM arc ratio s_2	0.85 - 1
Slot depth h_1 (mm)	14 - 18
PM height h_2 (mm)	3 - 5

Four design parameters, namely the slot opening-to-pitch ratio, slot depth, PM arc-to-pitch ratio, and PM thickness, are included in the x variables, with the ranges listed in Table II. A direct multi-search algorithm is implemented in Matlab for the multi-objective optimization to find the Pareto set of optimal solutions [10]. Fig. 7 shows the result of the Pareto set of optimal solutions, which represent the best solutions possible to maximizing torque without sacrificing power factor, and vice versa. The maximum achievable torque is over 280 N·m, which is over $1.8\times$ the rated torque of the benchmark SMPM motor, while the power factor is around 0.56; if higher power factor is preferred, we can also select design parameters that can achieve a 0.72 power factor, while the torque generation

V. Conclusions

We developed a subdomain-based analytical model for rapid evaluation of VPM motor performances, and validated the accuracy with nonlinear FEM simulations. We showed the trade-off between torque generation and power factor of the VPM motor, and implemented the analytical model for multi-objective optimization of a space-saving VPM motor for direct-drive application. In addition, the saturation effect was considered in the design optimization by setting threshold values of the stator flux density. With the analytical model based optimization strategy, other practical design considerations such as the active mass or the PM size can be included in the objective functions, and more design parameters can be included in the variables to be optimized.
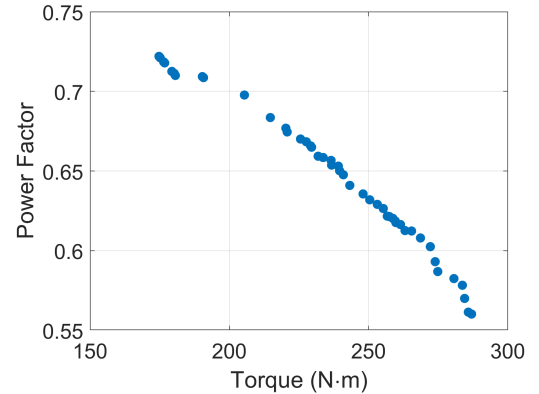

Fig. 7: The optimized Pareto front of torque and power factor.

is sacrificed. Such multi-objective optimizations allows us to select optimal designs depending on different requirements.

References

[1] R. L. Ficheux, F. Caricchi, F. Crescimbini, and O. Honorati, "Axial-flux permanent-magnet motor for direct-drive elevator systems without machine room," *IEEE Transactions on Industry Applications*, vol. 37, no. 6, pp. 1693–1701, 2001.

[2] A. Ishizaki, T. Tanaka, K. Takasaki, and S. Nishikata, "Theory and optimum design of pm vernier motor," 1995.

[3] B. Kim and T. A. Lipo, "Operation and design principles of a pm vernier motor," in *2013 IEEE Energy Conversion Congress and Exposition*. IEEE, 2013, pp. 5034–5041.

[4] D. Li, R. Qu, J. Li, L. Xiao, L. Wu, and W. Xu, "Analysis of torque capability and quality in vernier permanent-magnet machines," *IEEE transactions on industry applications*, vol. 52, no. 1, pp. 125–135, 2015.

[5] B. L. J. Gysen, K. J. Meessen, J. J. H. Paulides, and E. A. Lomonova, "General formulation of the electromagnetic field distribution in machines and devices using fourier analysis," *IEEE Transactions on Magnetics*, vol. 46, no. 1, pp. 39–52, 2010.

[6] B. Hannon, P. Sergeant, L. Dupré, and P. Pfister, "Two-dimensional fourier-based modeling of electric machines—an overview," *IEEE Transactions on Magnetics*, vol. 55, no. 10, pp. 1–17, 2019.

[7] Z. Q. Zhu, L. J. Wu, and Z. P. Xia, "An accurate subdomain model for magnetic field computation in slotted surface-mounted permanent-magnet machines," *IEEE Transactions on Magnetics*, vol. 46, no. 4, pp. 1100–1115, 2010.

[8] Y. Oner, Z. Q. Zhu, L. J. Wu, X. Ge, H. Zhan, and J. T. Chen, "Analytical on-load subdomain field model of permanent-magnet vernier machines," *IEEE Transactions on Industrial Electronics*, vol. 63, no. 7, pp. 4105–4117, 2016.

[9] K. Shin and B. Wang, "Semi-analytical modeling for interior permanent magnet synchronous machines considering permeability of rotor core," in *2020 23th International Conference on Electrical Machines and Systems (ICEMS)*, 2020, pp. 1–4.

[10] A. Custódio, J. Madeira, I. Vaz, and L. Vicente, "Direct multisearch for multiobjective optimization," *SIAM Journal on Optimization*, vol. 21, pp. 1109–1140, 07 2011.